Soft Matter

Accepted Manuscript

ROYAL SOCIETY OF CHEMISTRY

www.rsc.org/softmatter

DNA-PAMAM dendrimer complexes with structures similar to those in a nucleosome can form at low salt concentration, but have two different handedness when most dendrimer surface amine groups are nonacetylated.

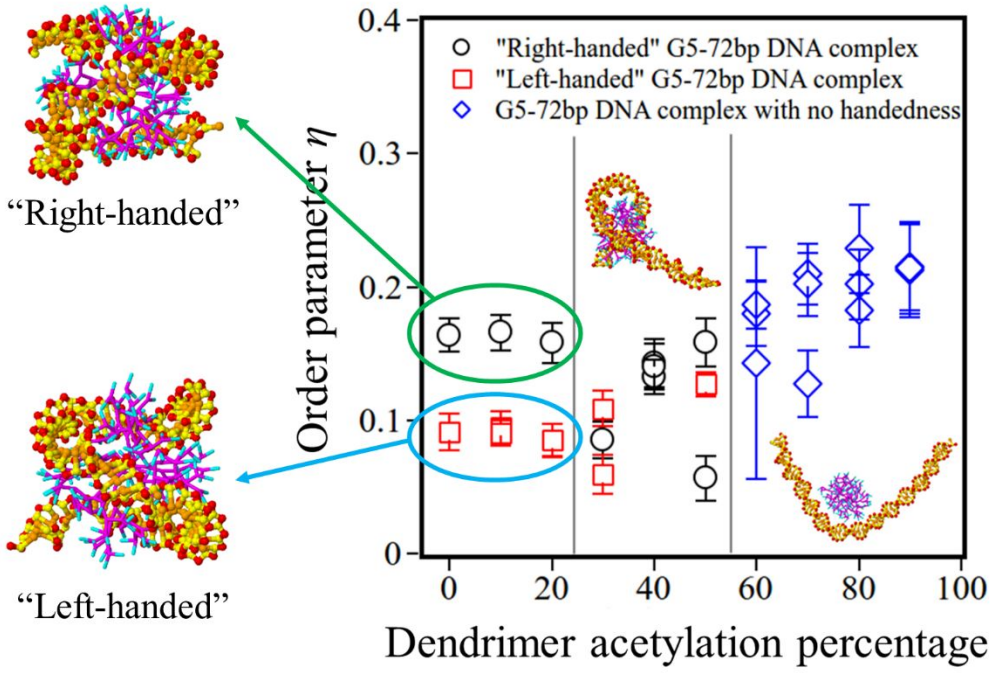

Monte-Carlo simulations of PAMAM dendrimer-DNA interactions

Shi Yu, Ronald G. Larson

Chemical Engineering Department,

University of Michigan, Ann Arbor 48109

ABSTRACT

We use Monte Carlo simulations to determine the influence of poly(amido amine) (PAMAM) dendrimer size and charge on its interactions with double-stranded DNA conformation and interaction strength. To achieve a compromise between simulation speed and molecular detail, we combine the coarse-grained DNA model of de Pablo et al.[1] which resolves each DNA base using three beads – and thereby retains the double-helix structure – with a dendrimer model with resolution similar to that of the DNA. The resulting predictions of the effects of dendrimer generation, dendrimer surface charge density, and salt concentration on dendrimer–DNA complexes are in agreement with both experiments and all-atom MD simulations. The model predicts that DNA wraps a fully charged G5 or G6 dendrimer at low salt concentration (10 mM) similarly to a histone octamer, and for the G5 dendrimer, DNA super helices with both handednesses occur. At salt concentrations above 50 mM, or when a high fraction of dendrimer surface charges are neutralized by acetylation, DNA adheres but does not compactly wrap the dendrimer, in agreement with experimental findings. We are also able to simulate pairs of dendrimers binding to the same DNA strand. Thus, our mesoscale simulation not only elucidates dendrimer-DNA interactions, but also provides a methodology for efficiently simulating chromatin formation and other cationic macroion – DNA complexes.

1. Introduction

Extensive experimental studies, e.g., cryo-TEM,[2,3] small angle X-ray scattering,[4] and dynamic light scattering,[5,6] have recently been performed to investigate the size and morphology of complexes of cationic poly(amido amine) (PAMAM) dendrimer with double-stranded DNA. This interest is driven by the ability of this dendrimer to condense dsDNA, opening up possible applications in gene delivery.[7,8] Since the strongest interaction between cationic dendrimers and DNA is electrostatic, the size as well as the morphology of the complex are highly dependent on salt concentration,[9] pH,[4] and dendrimer surface groups.[10] Therefore, a dendrimer – DNA model that captures the electrostatic interaction correctly, and with appropriate resolution, would stimulate deeper understanding of the physical properties of the complexes and help in the design of novel dendrimers for gene delivery. In addition, dendrimers of generation 5 or larger are roughly comparable in size to histone octamers and so can model DNA-histone interactions, and help in understanding DNA-protein interactions more generally.

However, accurate all-atom molecular dynamics (AAMD) simulations can only be applied routinely to fairly small dendrimer – DNA systems,[11,12] since AAMD simulations are computationally expensive. On the other hand, widely used coarse-grained (CG) models,[13–16] which use bead-spring or bead-rod chains to model dsDNA as an effectively single-strand linear polyelectrolyte, can simulate binding and wrapping of DNA around a dendrimer. However since the diameter of dsDNA is almost the same as the radius of the dendrimer, the double-helix structure of DNA might be critical for local arrangement of the DNA along the dendrimer surface and thereby strongly affect the structure of the dendrimer – DNA complex. To the best of our knowledge, only the recent work of Cao et al.,[17] which employs Savelyev and Papoian's double stranded coarse-grained DNA model,[18] discusses how a double helix polyelectrolyte can

be captured by a charged nanosphere, thus providing a simplified model of DNA condensation by a macroion. Note that in Savelyev and Papoian's DNA model, DNA melting and sequence-dependent bending were not allowed and a hard sphere with hundreds of charges evenly distributed over its surface was used for the macroion. Such a model, while useful especially for DNA condensation by hard, uniform nanoparticles, does not describe details of local DNA structures adsorbed to flexible nanoparticles such as dendrimers, and cannot describe local DNA melting. To study DNA local bending and melting caused by strong attractions between a dendrimer and DNA, a finer-scale, yet still coarse-grained, DNA model is necessary, one that captures the double helix structure of dsDNA, allowing DNA double strand super-coiling, melting and re-association. Such a model, called the "3SPN" coarse-grained model, was developed by de Pablo and co-workers, [1,19,20,21] in which a single bead represents each of the phosphate, sugar, and bases, reducing the number of degrees of freedom significantly relative to atomistic models. Moreover, this "3SPN" model can generate accurate DNA sequence-dependent melting curves as well as an accurate persistence length for double stranded DNA. Thus, the 3SPN model makes it easily affordable to study the interactions of a relatively long strand of dsDNA (e.g., 144 bp) with dendrimers of various generations without sacrificing the DNA local double helical structure. Another main advantage of the 3SPN model is that the electrostatic force is treated using the Debye-Hückel theory which can easily be adapted (as we do here) to compute the electrostatic interactions with other molecules, in particular, charged dendrimers. However, since the 3SPN model is based on the classical B-form dsDNA structure, Hogsteen interactions are not included in this DNA model.

It is worth mentioning that a CG model that incorporates both this 3SPN DNA model and a CG dendrimer model with similar resolution has not heretofore been published. Thus, here, we

combine the charged bead-spring dendrimer model of Muthukumar and coworkers[13] with the 3SPN DNA model by choosing an appropriate repulsive force between DNA and dendrimer beads that leads to a good match to the free energy of dendrimer – DNA binding found in all-atom MD simulations.[12] As will be discussed below, the combination of Muthukumar and dePablo model does not significantly disrupt the local double helix structure of the DNA.

Using this coarse-grained model, which we call the 3SPN-WM (Welch, Muthukumar[13]) model, we seek to study systematically DNA-dendrimer complex formation as a function of dendrimer generation, dendrimer surface charge density, and salt concentration, and to validate our coarse-grained model by comparing these simulation results to our previous experimental work.[6] Our coarse-gained model could also be extended to describe other DNA – macroion complexes, such as the DNA – histone complex, which is of great biological importance. Compared to recent coarse-grained models of DNA – histone complexes,[22–24] our new coarse-grained model presented here should give more detailed information regarding sequence-dependent bending of DNA for relatively long DNA sequences (>146 bp). Hence, our dendrimer – DNA (3SPN-WM) model is not only of interest in its own right, but is a good starting point for developing a new CG model of the DNA – histone complex which can bridge the gap between an all-atom model and a simpler bead-spring model of this complex.[22] Such a CG model can help in the design of dendrimers with optimal surface charge density, which might increase transfection efficiency.

2. Simulation model and method

Dendrimer model

In this paper, a PAMAM dendrimer with an ethylenediamine core was modeled by a bead-spring, so-called "united-atom" model.[13] An ethylenediamine (EDA) core PAMAM dendrimer has 33% more terminal groups than the same-generation ammonia-core PAMAM dendrimer

simulated by Welch and Muthukumar[13], and thus is less flexible than the ammonia-core dendrimer. For an ethylenediamine-core dendrimer, the relationship between the number of dendrimer beads (N_D) in the CG model and the dendrimer generation number (G) is:

$$N_D = N_{interior} + N_{terminal} = (2^{G+2} - 2) + 2^{G+2} \quad (1)$$

where $N_{interior}$ and $N_{terminal}$ are the number of interior and terminal beads, respectively. Fig. 1 shows how a generation 1 (G1) dendrimer is modeled, where the interior and terminal beads are rendered in magenta and cyan, respectively. The mass of each bead is 113 (amu). (Assignment of specific atoms to CG beads of each color in Fig. 1 was not attempted, and bending and torsional potentials were not included in the dendrimer model, although they are present in the DNA model of de Pablo and coworkers; see Eqs 8~14.) The CG model of an ammonia-core dendrimer by Welch and Muthukumar contains only a single bead at the center, attached to three branches, rather than the pair of beads attached to four branches for the ethylenediamine-core dendrimer depicted in Fig. 1. Apart from this difference, the CG model used here is identical to that of Welch and Muthukumar.[13]

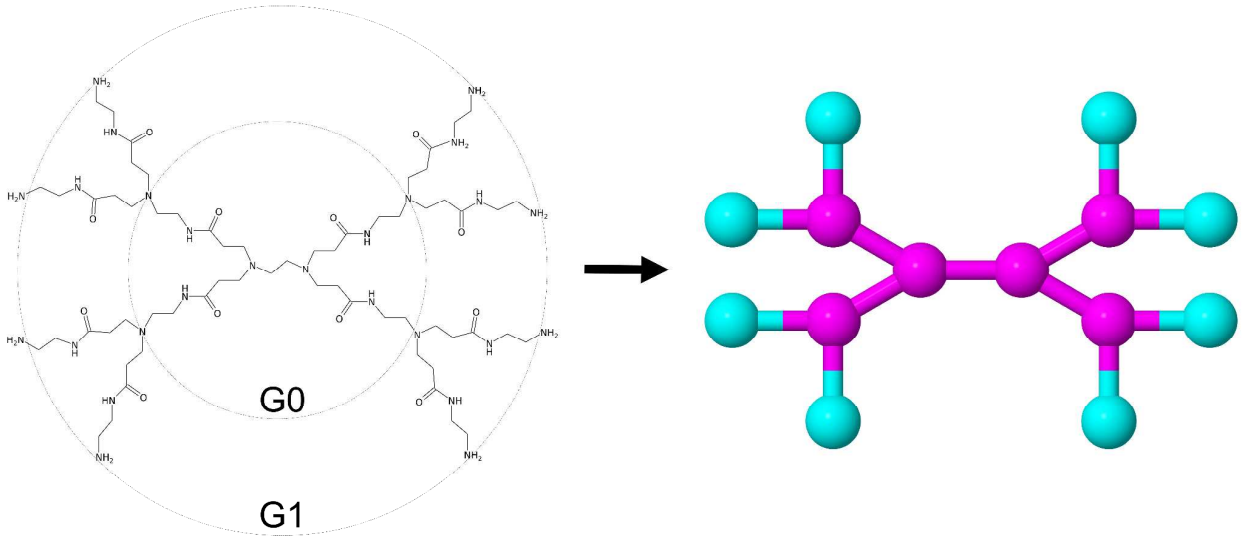

Fig. 1 Depiction of the bead-spring model for a generation 1 (G1) PAMAM dendrimer. This, and other molecular depictions, were generated using Jmol: an open-source Java viewer for chemical structures available at 3D. http://www.jmol.org/.

Here, we include only three forces: bond stretching, excluded volume, and Coulombic. As described in Ref. 13, we used the finitely extensible nonlinear elastic" (FENE) force to model the bond stretching energy (Eq. 2).

$$\frac{U_{FENE}}{k_B T} = -KR^2 \sum_{i=1}^{N_D} \log\left[1 - \left(\frac{l_i - l_0}{R}\right)^2\right] \tag{2}$$

where U_{FENE} is the total bond stretching energy for the dendrimer; K, set to $20.0/l_0^2$, is the spring constant; and l_i is bond length of the *ith* bond. Also $l_0 = (l_{\max} + l_{\min})/2$, where $l_{\max}$ and $l_{\min}$ are the maximum and minimum bond lengths respectively, and $R = l_{\max} - l_0$. In all our simulations, $l_{\max}$ was set to $1.0l_{B,}$ and $l_{\min}$ to $0.4l_B$, where l_B is the Bjerrum length (Eq. 5) which is 7.1 Å at 25 °C in water which are the same values as used by Welch and Muthukumar[13]. N_D is the number of dendrimer beads.

The electrostatic repulsion force between the charged dendrimer terminal beads is computed using the Debye-Hückel potential: [13] (Eqs. 3-5 explicitly demonstrate that the electrostatic interaction terms from de Pablo et al. and from Welch and Muthukumar are identical. The second term in Eq. 3 was used in the work of de Pablo et al., while the third term was used in Welch and Muthukumar)

$$\frac{U_{elec}}{k_B T} = \sum_{i<j}^{N_T} \frac{q_i q_j e_c^2 e^{-\kappa r_{ij}}}{4\pi\epsilon_0 \epsilon(T,C) r_{ij} k_B T} = l_B \sum_{i<j}^{N_T} \frac{q_i q_j e^{-\kappa r_{ij}}}{r_{ij}} \tag{3}$$

where U_{elec} is the electrostatic energy and κ is inverse Debye length, which is defined by:

$$\kappa^{-1} = \sqrt{\frac{\epsilon_0 \epsilon(T,C) k_B T}{2 N_A e_c^2 I}} \quad (4)$$

The Bjerrum length l_B is given by:

$$l_B = \frac{e_c^2}{4\pi\epsilon_0 \epsilon(T,C) k_B T} \quad (5)$$

Here r_{ij} is the distance between the ith and jth beads and q_i and q_j are the number of charges on the ith and jth beads, respectively. N_A is Avogadro's number; ϵ_0 is the vacuum permittivity, and $\epsilon(T,C)$ is the temperature (T) and salt-concentration (C)-dependent dielectric constant. Since all the simulations were carried out at 25 °C, the dielectric constant only depends on salt concentration. The definition of $\epsilon(T,C)$ can be found somewhere else[25]. e_c and I are the elementary charge and ionic strength, respectively. N_T is the number of charged terminal groups on the dendrimer.

To avoid overlapping of dendrimer beads, the excluded volume potentials between all dendrimer beads were computed using the Morse potential [13], as shown in Eq. 6:

$$\frac{U_{Morse}}{k_B T} = \frac{\sigma}{k_B T} \sum_{i<j}^{N_D} \left[\left(e^{-\alpha(r_{ij}-d)} - 1 \right)^2 - 1 \right] \quad (6)$$

where $\sigma = k_B T / 0.7$; $\alpha^{-1} = l_B / 24$ and $d = 0.8 l_B$. Again, N_D is the total number of dendrimer beads. For r_{ij}>9 Å, the excluded volume potential was cut off.

DNA model (3SPN.1 force field)

We used the coarse-grained model of dsDNA developed by de Pablo and coworkers[19,1] (3SPN.1 force field) to simulate the DNA. For completeness, we list below all equations used. The constants used in these equations and further details about this force field can be found in the original papers[19,1].

The bonded interactions of the 3SPN.1 force field are given by:

$$\frac{U_{bond}}{k_B T} = \beta \sum_{i=1}^{n_{bond}} \left[k_1 (d_1 - d_{0i})^2 + k_2 (d_1 - d_{0i})^4 \right] \tag{7}$$

$$\frac{U_{bend}}{k_B T} = \beta \sum_{i=1}^{n_{bend}} \frac{k_\theta}{2} (\theta_i - \theta_{i0})^2 \tag{8}$$

$$\frac{U_{tors}}{k_B T} = \beta \sum_{i=1}^{n_{tors}} k_\phi [1 - \cos(\phi_i - \phi_{i0})] \tag{9}$$

Here U_{bond}, U_{bend}, and U_{tors} represent bond stretch energy, bending energy, and dihedral energy respectively, with $\beta = 1/k_B T$. The nonbonded, pairwise interactions between DNA beads are given by:

$$\frac{U_{stck}}{k_B T} = \beta \sum_{i<j}^{n_{stck}} 4\varepsilon \left[\left(\frac{\sigma_{ij}}{r_{ij}} \right)^{12} - \left(\frac{\sigma_{ij}}{r_{ij}} \right)^{6} \right] \tag{10}$$

$$\frac{U_{base}}{k_B T} = \beta \sum_{i=1}^{n_{base}} 4\varepsilon_{bi} \left[5 \left(\frac{\sigma_{bi}}{r_{ij}} \right)^{12} - 6 \left(\frac{\sigma_{bi}}{r_{ij}} \right)^{10} \right] \tag{11}$$

$$\frac{U_{nnat}}{k_B T} = \beta \sum_{i<j}^{n_{nnat}} \begin{cases} 4\varepsilon \left[\left(\frac{\sigma_0}{r_{ij}} \right)^{12} - \left(\frac{\sigma_0}{r_{ij}} \right)^{6} \right] + \varepsilon & \text{if } r_{ij} < r_{coff} \\ 0 & \text{if } r_{ij} \geq r_{coff} \end{cases} \tag{12}$$

$$\frac{U_{elec}}{k_B T} = \sum_{i<j}^{N_{elec}} \frac{q_i q_j e_c^2 e^{-\kappa r_{ij}}}{4\pi\epsilon_0 \epsilon(T,C) r_{ij} k_B T} = l_B \sum_{i<j}^{N_{elec}} \frac{q_i q_j e^{-\kappa r_{ij}}}{r_{ij}} \tag{13}$$

$$\frac{U_{solv}}{k_B T} = \beta \sum_{i<j}^{n_{solv}} \varepsilon_S \left[1 - e^{-\alpha' (r_{ij} - r_S)} \right]^2 - \varepsilon_S \tag{14}$$

Both the base-stacking effects (U_{stck}), and the intra-strand interaction and hydrogen-bonding interactions between DNA complementary base pairs (U_{base}) contribute to the stiffness of the DNA double-strand helix. A complementary base-pair is considered to be hydrogen-bonded only when the distance between those two base beads is less than (σ_{bi}+2.0 Å). The excluded volume

potential between DNA beads was included in the nonnative contact potential U_{nnat}. The electrostatic repulsions between DNA phosphate beads were calculated from a Debye-Hückel potential, as is the case with charged dendrimer beads; i.e., Eq. 13 is the same as Eq. 3. The solvent-induced energy U_{solv} was used to capture electrostatic correlation effects along the DNA[26]. A complete description of how to determine the parameters and DNA related potentials can be found in Sambriski et al[1].

Dendrimer-DNA interaction

Since the attractive force between DNA and the PAMAM dendrimer is dominated by electrostatic interactions,[11] for simplicity, we only considered two different forces between DNA and dendrimer beads, namely the electrostatic and excluded volume forces. We again used the Debye-Hückel potential to model the electrostatic attraction between DNA and dendrimer beads (Eq. 15). Compared to the dendrimer and DNA macroions, the salt ions and water molecules are small enough that an implicit model for their effect hopefully provides an adequate description.

$$\frac{U_{elec}}{k_B T} = \sum_{i=1}^{N_T}\sum_{j=1}^{N_P} \frac{q_i q_j e_c^2 e^{-\kappa r_{ij}}}{4\pi\epsilon_0 \epsilon(T,C) r_{ij} k_B T} = l_B \sum_{i=1}^{N_T}\sum_{j=1}^{N_P} \frac{q_i q_j e^{-\kappa r_{ij}}}{r_{ij}} \tag{15}$$

Note N_P here is the number of charged DNA beads, that is, the number of phosphate beads. Eq. 15 is the same as Eqs. 3 and 13, except that it is summed over only the cross-interactions between a DNA bead with a dendrimer bead.

The excluded volume potential between PAMAM dendrimer beads and DNA beads was modeled by a truncated Lennard-Jones potential:

$$\frac{U_{excluded}}{k_B T} = \beta \sum_{i=1}^{N_D}\sum_{j=1}^{N_{DNA}} \begin{cases} 4\varepsilon\left[\left(\frac{\sigma'}{r_{ij}}\right)^{12} - \left(\frac{\sigma'}{r_{ij}}\right)^{6}\right] + \varepsilon & \text{if } r_{ij} < r_{cutoff} \\ 0 & \text{if } r_{ij} \geq r_{cutoff} \end{cases} \text{Error! Reference source not found.}$$

(16)

where $\sigma' = 2^{-1/6} r_{cutoff}$ where ε in the above takes the same value as assigned to this symbol in Eqs. 10 and 12. To determine r_{cutoff}, we compared the potential of mean force (PMF) computed from our CG model for a generation 3 (G3) PAMAM dendrimer interacting with a 24 base pair dsDNA (Figure 4a) with the corresponding PMF for the interaction of these molecules from an all-atom molecular dynamics simulation.[12] The DNA base pair sequence used in these simulations is CGCGAATTCGCGCGCGAATTCGCG[12,27].

Simulation methods

We employed a Monte-Carlo simulation method in a canonical ensemble using the classical Metropolis sampling method to simulate the CG DNA-PAMAM dendrimer interaction. The trial displacements of each bead Δx, Δy, Δz were randomly distributed uniformly within the range (-0.35Å, 0.35Å). The acceptance probability of our simulation was around 33%. Note we use an implicit solvent model, and periodic boundary conditions were not used.

For our umbrella sampling simulations, the reaction coordinate was defined as the distance between the dendrimer center of mass and the center of mass of the two base pairs in the middle of the 24 bp DNA. A harmonic potential with a force constant of 0.25 kcal/mol/Å^2 was applied along the reaction coordinate over each of 90 successive windows in 1-Å increments. Force constants of 0.5 kcal/mol/Å^2 were also used for limited runs, and showed similar results to those obtained with a constant of 0.25 kcal/mol/Å^2. For each window, the system was equilibrated for 3×10^6 Monte Carlo steps (MCS), where a single step consists of an attempt to move a single bead. Larger force constants (e.g., above 1 kcal/mol/Å^2) resulted in poorer overlap of the histograms, which caused bigger errors for the specific simulation time used here. The potential of mean force (PMF) was obtained using the weighted histogram analysis method (WHAM).[28]

3. Results and discussion

3.1 PAMAM dendrimer simulations

As described above, we use the dendrimer model of Welch and Muthukumar[13] to simulate a PAMAM dendrimer with an ethylenediamine (EDA) core. To test the suitability of the model, we report here the radii of gyration (R_g) of EDA-core dendrimers of generations G3 through G6, and for G5 dendrimers acetylated to different extents. The largest dendrimer that we simulate (G6) is represented by 510 beads.

Dendrimer generation and salt concentration effects. As shown in Fig. 2, G3-G6 PAMAM dendrimers show a 12% (G3) to 21% (G6) decrease in the radius of gyration (R_g) as the salt concentration increases from 10 to 1,000 mM. As expected, dendrimers of higher generation shrink more as salt concentration increases, and repulsive forces of charged terminal groups are reduced by ion screening. Table 1 compares values of R_g from our simulations with those from small angle x-ray scattering (SAXS) experiments and from molecular dynamics simulations. The good agreement shows that the CG model of Welch and Muthukumar can be used to obtain the correct size of the EDA-cored PAMAM dendrimers considered here, as well as the ammonia-core dendrimers considered by Welch and Muthukumar.

Note that increasing salt concentration has similar effects on dendrimer size as does increasing pH, since at high pH only a fraction of the dendrimer terminal amine groups is protonated, which weakens the repulsion between these terminal groups relative to those with fully charged surface groups at low pH. However, the molecular dynamics simulations of a G4 dendrimer by Liu et al.[29] show only a 4.9% decrease in R_g when the pH increases from low (5) to high (>10).

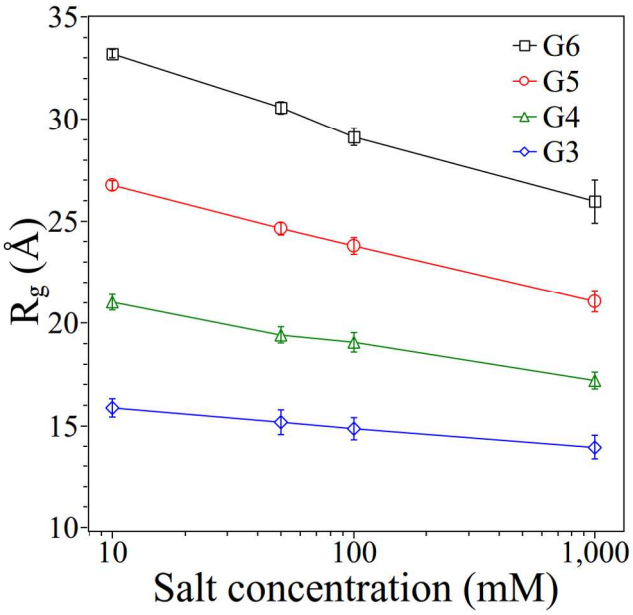

Fig. 2 Radii of gyration of PAMAM dendrimers as a function of salt concentration. (The error bars are standard deviations).

TABLE 1~~1~~ Radii of gyration R_g (in Å) for EDA-core PAMAM dendrimers[a]

Dendrimer generation	Number of beads	Total number of charges	Radius of gyration (R_g)			
			this work 1M [Na^+]	Maiti et al.[30,31]	Lee et al.[32]	SAXS[33]
G3	62	32	13.94±0.60	11.23[30]		15.8
G4	126	64	17.19±0.41	17.01±0.10[31]		17.1
G5	254	128	21.05±0.52	22.19±0.14[31]	25.1±0.1	24.1
G5-90%Ac	254	13.7±4.0	20.78±0.37		21.1±0.1	
G6	510	256	25.96±1.06	27.28±0.39[31]		26.3

[a] Debye length in a 1M [Na^+] solution is 3 Å. The R_g values from the work of Maiti et al.[30,31] were obtained at high salt concentration with Debye length equal to 4.3 Å. The R_g values from Lee et al.[32]were obtained by MD simulations with no salt. SAXS experiments were carried out in methanol solutions.

Acetylation effects. The surface charge density of a dendrimer affects its ability to condense DNA as well as its cytotoxicity. For example, a dendrimer with a higher surface charge density has a higher transfection efficiency,[34] but could be more cytotoxic as it can generate pores on the cell membrane. Thus, adjusting the dendrimer charge density by surface modifications such as PEGylation or acetylation is of great interest. Since we adopted a coarse-grained dendrimer

model and the acetyl functional group is small compared to the size of dendrimer CG beads, we simulate the acetylated dendrimer simply by randomly assigning zero charges to some of the terminal beads of the dendrimer. The R_g of the resulting acetylated dendrimers are plotted against percentage acetylation in Fig. 3. For each degree of acetylation, three runs at 10 mM salt concentration were averaged together. For a low degree of acetylation (<50%), R_g decreases almost linearly. For higher degrees of acetylation, a near-plateau in dendrimer size is eventually attained. A fully neutralized G5 dendrimer has a 22% smaller radius of gyration than a non-acetylated dendrimer, which is a somewhat greater reduction than shown by corresponding atomistic MD simulations (~16%). [32]

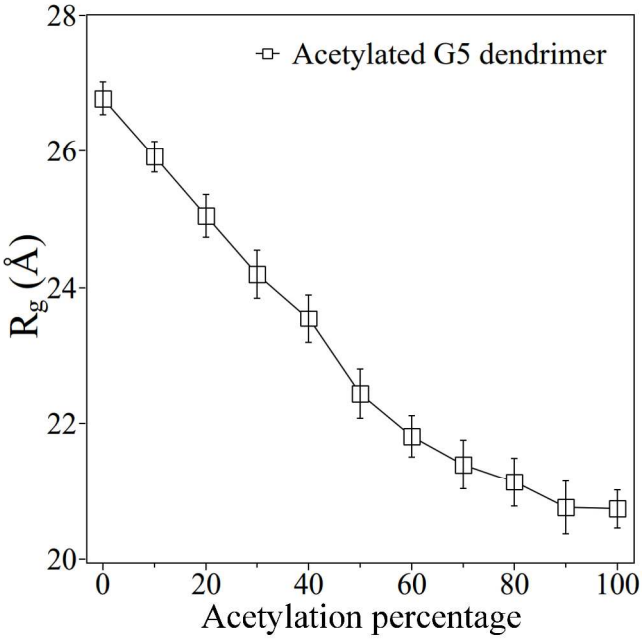

Fig. 3 Radius of gyration of PAMAM dendrimer as a function of acetylation percentage. (The error bars are standard deviations).

3.2 DNA simulations

We verified our code by simulating a 38 bp dsDNA and comparing its persistence lengths at different salt concentrations to the results of de Pablo and coworkers,[1] using the same method

described in their paper. The persistence length in that paper was defined by $\langle \hat{u}(0)\cdot\hat{u}(s)\rangle = e^{-s/l_p}$, where $\hat{u}(s)$ is the unit tangent vector at relative position s along the DNA, and l_p is the persistence length. Since different persistence length formulas give different results for macromolecular chains,[35] we only compare our persistence length results to those of de Pablo et al. Our DNA sequence is chosen to be the same as that used by Nandy and Maiti [11]. The results are presented in table 2 (f_{CG} is CG content of DNA), which agree with the results of de Pablo and coworkers. The increase in persistence length (l_p) of DNA when salt concentration is reduced to 10 mM is caused by the stronger repulsions between phosphate beads of DNA. Because obtaining l_p using Monte-Carlo (MC) simulations is computationally expensive, we do not obtain l_p for longer DNA using our MC code.

TABLE 22 List of DNA simulations and persistence length determinations

N_{nt}	f_{CG}	Base pair sequence (5′ to 3′)	[Na^+] (M)	l_p (nm)
			0.150	43±3
38	0.659	GCCGCGAGGTGTCAGGGATTGCAGCCAGCATCTCGTCG	0.100	39±6
			0.010	74±2

3.3 Potential of mean force (PMF) of dendrimer – DNA binding

The free energy change or potential of mean force (PMF) of a G3 PAMAM dendrimer binding to a 24-bp DNA molecule was obtained by umbrella sampling and the results are plotted in Fig. 4b. The PMFs were used for parameterization of the dendrimer – DNA interaction. Specifically, we compared the PMFs from our CG model with various excluded volume cut-off distances (defined in Eq. 16) to results from all-atom MD (AAMD) simulations.[12] We then chose a cut-off distance giving good agreement to the PMF from the AAMD simulations for the G3-DNA interaction, and used this for higher generation dendrimers as well, since the dendrimer terminal groups were the same and were represented by the same bead type regardless of the generation.

However, to confirm that this potential is adequate for other generations of dendrimer, structural parameters such as the radius of gyration of the DNA-dendrimer complex should also be compared to results from AAMD simulations. As shown in Fig. 4b, when r_{cutoff} = 10 Å, the minimum of the PMF curve is located between 20 and 30 Å, and free energy change of binding reaction is -10 kcal/mol, which agree well with AAMD results (-10.9~-13.5 kcal/mol).[12] Therefore, here we use r_{cutoff} = 10 Å for all our simulations. The large difference between the curves in Fig. 4b indicates that the binding free energy is very sensitive to this cut-off, r_{cutoff}. This sensitivity arises from the strong distance dependence of the electrostatic interactions between dendrimer and DNA beads. The simple cut-off scheme is chosen, despite the sensitivity to the cut-off parameter, because our coarse-grained model cannot capture the atomic-level interactions that determine the actual local structure. Hence we use a cut-off tuned to ensure that at least we obtain the same PMF as is found in the all-atom simulations, so that model correctly the net attractive interaction between DNA and dendrimer.

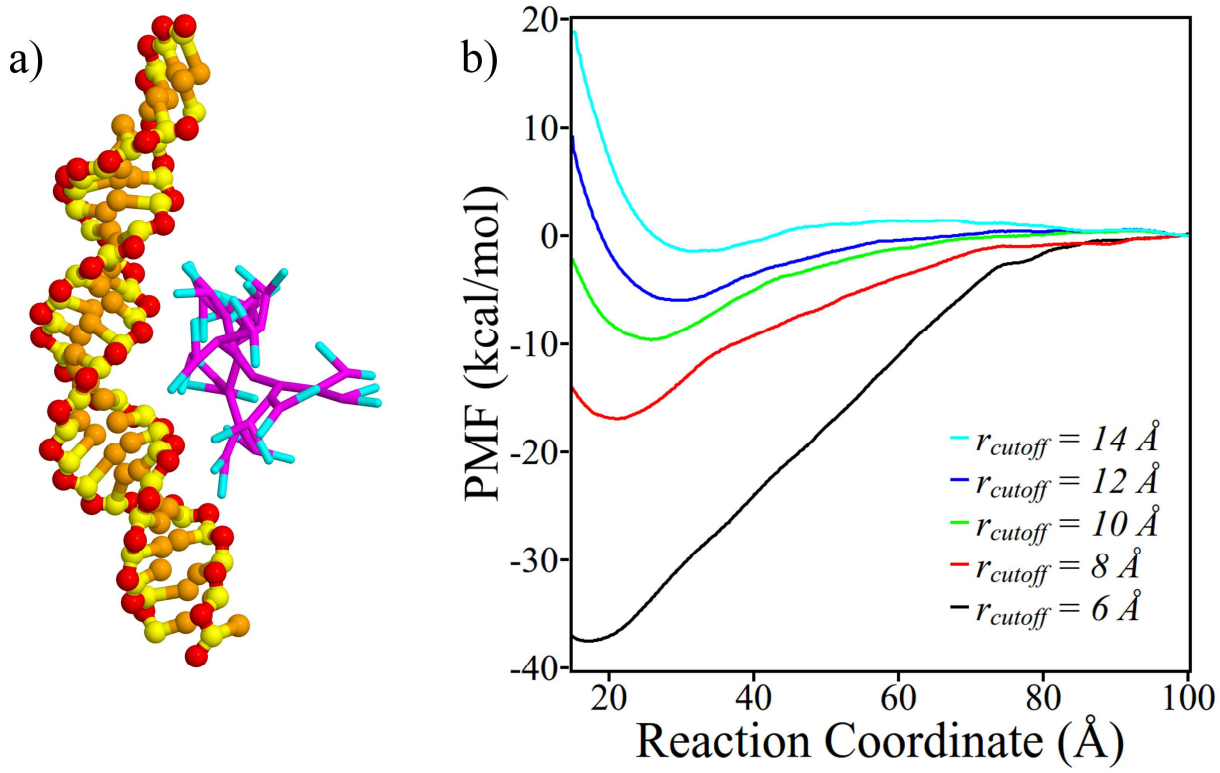

Fig. 4 a) Image of G3 PAMAM dendrimer binding a 24 bp DNA. b) Corresponding potential of mean force (PMF) curves for different cutoff distances (r_{cutoff}).

3.4 PAMAM dendrimer – DNA complex formation

Snapshots of a 144 bp dsDNA binding to a G6 dendrimer are shown in Fig. 5. Since all our simulations were carried out using a Monte-Carlo simulation method, this binding process does not necessarily show the actual dynamics but only one path to the final structure. A G6 dendrimer is of similar size and charge density to a histone octamer. Therefore, just as histones do not form the classical nucleosome structures with DNA at salt concentrations as low as 10 mM, a G6 dendrimer attracts DNA too strongly for an equilibrium complex structure to be achieved. The dendrimer – DNA complex shown in Fig. 5c is only one of the multiple metastable structures we obtained in our simulations (others not shown) after simulations up to 1.6×10^7 Monte Carlo steps (MCS). While the structure in Fig. 5c is a right-handed helix, others

have different handedness, or disordered structures. These metastable structures are sufficiently long-lived that their properties, such as R_g, could be averaged over a long enough time to obtain meaningful results. Since dendrimer-DNA complex formation might also be kinetic-controlled in experiements,[5] the metastable structures determined here by simulation might provide physically realistic structural information of the complexes. In the simulation depicted in Fig. 5, we used the same 144 DNA base-pair sequence given elsewhere.[1]

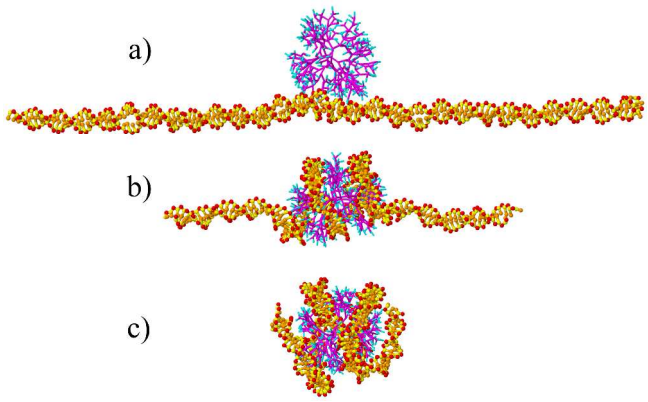

Fig. 5 Snapshots of 144bp dsDNA – G6 dendrimer interaction at 10 mM salt concentration: a) after 6×10^4 MCS, b) after 6×10^6 MCS, c) after 1.6×10^7 MCS.

Effects of dendrimer generation and salt concentration

To further validate our CG model, we investigated the condensation of a 38 bp DNA (see Table 2) by G3, G4, and G5 dendrimers at various salt concentrations and compared the results to those of AAMD simulations[11] directly. We define r_{charge} by Eq. 17:

$$r_{\text{charge}} = \frac{\text{number of positive charges on dendrimer}}{\text{number of negative charges on DNA}} \qquad (17)$$

Note that r_{charge} is less than unity for G3 – 38bp DNA and G4 – 38 bp DNA complexes but larger than unity for the G5 – 38 bp DNA complex. We also simulated a G5 – 72 bp DNA complex, for which $r_{\text{charge}} < 1$. The base-pair sequence of the 72 bp DNA is the same as the central 72 base-pairs of the 144 bp DNA discussed above. We limited ourselves primarily to $r_{\text{charge}} < 1$ to study

DNA condensation by dendrimers rather than decoration of DNA by dendrimers. The effects of dendrimer generation and salt concentration on complex formation are summarized in Fig. 6-9.

As shown in Fig.6, a DNA molecule wraps around a dendrimer tightly at low salt concentration (10 mM), but is much straighter at high salt concentration (100 mM), due to the stronger ion screening effects at higher salt concentration. On the other hand, for a given salt concentration the DNA compacts more tightly with a higher generation dendrimer. Therefore, a high generation dendrimer at high salt concentrations behaves like a lower generation dendrimer at lower salt concentration, in agreement with observations by cryo-TEM.[9] (Unlike the larger dendrimer-DNA complex (G6-144bp DNA), the specific structures in Fig.6 can be achieved in repeat runs.)

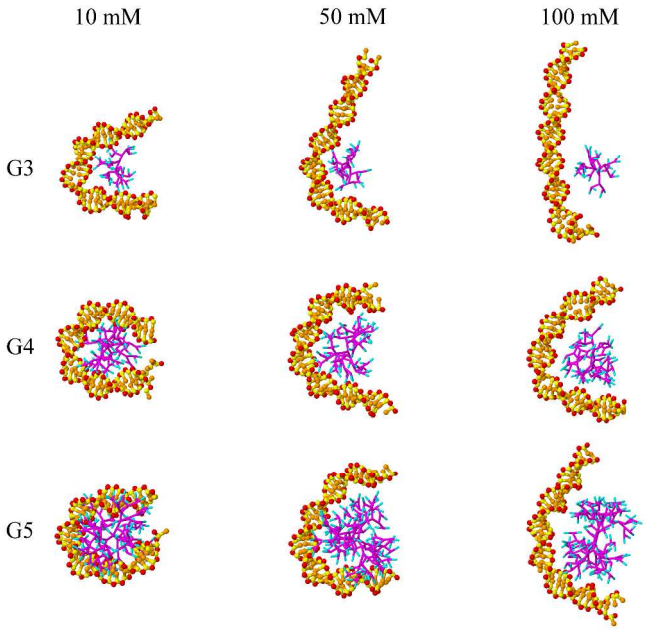

Fig. 6 38 bp DNA condensed by G3, G4, and G5 dendrimers at salt concentrations of 10, 50, and 100 mM.

Radii of gyration (R_g) of complexes and of the dendrimers and DNA molecules within those complexes are plotted in Fig. 7. Error bars in Fig. 7 are the standard deviations of R_g from 500

sampling points where bead coordinates were recorded every 1×10^4 MCS after 5×10^6 MCS equilibration. Our R_g results for G4/G5 dendrimer-38bp DNA complexes at 10 mM salt concentration are similar to the AAMD results[11], which further validates our CG model of the dendrimer – DNA interaction. AAMD simulation results for longer DNA dendrimer complexes are unavailable. Note that the R_g values of these complexes are very sensitive to the salt concentration. The R_g of the dendrimer alone increases monotonically when salt concentration is reduced because the electrostatic repulsion within the dendrimer molecule becomes stronger. But the R_g of the DNA in the complex and the R_g of complex itself both decrease monotonically with decreasing salt concentration because of increased attraction between DNA and dendrimer at the lower salt concentration. And for 10 mM salt, even a G3 dendrimer is able to condense a 38 bp DNA significantly.

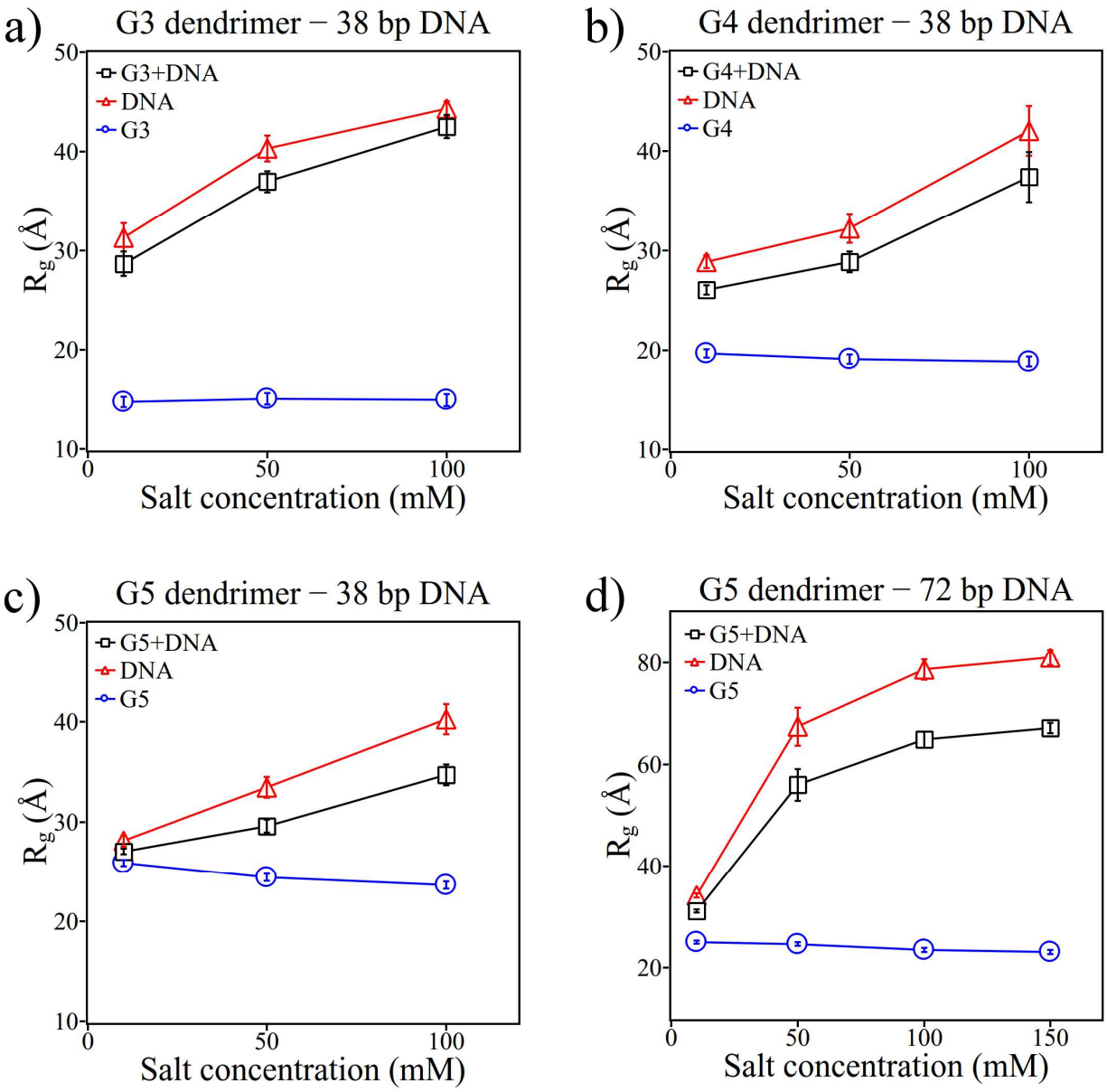

Fig. 7 R_g of complexes (black) as well as of dendrimers (blue) and DNA molecules (red) within those complexes as functions of salt concentrations. a) G3 – 38 bp DNA, b) G4 – 38 bp DNA, c) G5 – 38 bp DNA, d) G5 – 72 bp DNA. (The error bars are standard deviations).

The fractions of DNA phosphate beads adsorbed to the dendrimer surfaces for different complexes are plotted in Fig. 8a. An "adsorbed" DNA phosphate bead is defined as one whose distance to the nearest dendrimer bead is less than $l_B+r_{cutoff} = 17.1$ Å. As shown in Fig. 8a, the adsorption in all four complexes decreases monotonically with increasing salt concentration, as

expected. To quantify the arrangement of adsorbed DNA segments on the dendrimer surface, we use a curvature order parameter η[17,36] defined by:

$$\eta = \frac{\left| \sum_{\langle i \rangle} \bar{r}_{i,i+1} \times \bar{r}_{i+1,i+2} \right|}{N_d} \tag{18}$$

where $\bar{r}_{i,i+1} = \frac{r'_{i,i+1}}{\left| r'_{i,i+1} \right|}$, $r'_{i,i+1} = r'_{i+1} - r'_i$, $r'_i = \left(r_i + r_{i+n_{base}} \right)/2$, N_d is the number of adsorbed DNA phosphate bead pairs, n_{base} is the total number of base pairs of the DNA, r_i is the ith phosphate bead position, and $r_{i+n_{base}}$ is the phosphate bead position of the complementary base. Note that Eq. (18) only accounts for the cross product of adjacent vectors $\bar{r}_{i,i+1}$ and $\bar{r}_{i+1,i+2}$ for which the ith, (i+1)th, (i+2)th base pairs were all adsorbed onto the dendrimer (the ith base pair was considered as "adsorbed" when either ith or $i+n_{base}$ phosphate bead was adsorbed onto the dendrimer). The order parameter defined in Eq. 18 is zero when the DNA conformation is straight, and when it is randomly coiled. The curvature order parameter would be unity if the backbone of the DNA were to bend an angle of 90° at each basepair, always in the same direction, forming a tight helix. This order parameter was originally designed for a single-strand helix-forming molecule,[34] and when applied to each strand of a straight dsDNA molecule, taking the position vectors to be phosphates, yields an order parameter of η = 0.4271. For straight B-form dsDNA with position vectors taken to be the midpoints between the paired phosphate beads as assumed in Eq. 18, the order parameter is nearly zero (η = 0.0076494).(For the dsDNA, the order parameter defined in Eq. 18 describes supercoiling of double strand DNA.)

Disordered complexes, where the DNA chain is adsorbed to the dendrimer surface randomly, produce small values of the order parameter η (e.g., <0.05[17]). Our results (Fig. 8b) shows that the

degree of DNA order decreases with decreasing salt concentration, due to more severe bending of DNA at low salt concentrations. The error bars in Fig. 8 are standard deviations over 500 sampling points, which were taken every 1×10^4 MCS after equilibration. The standard deviation in the order parameter is much larger than of the adsorption fraction because there are many microstates with similar adsorption fraction but quite different order parameter, since the system energy is mainly controlled by the electrostatic attraction. The standard error of the mean is much smaller than the standard deviations shown by the error bars in Fig. 8.

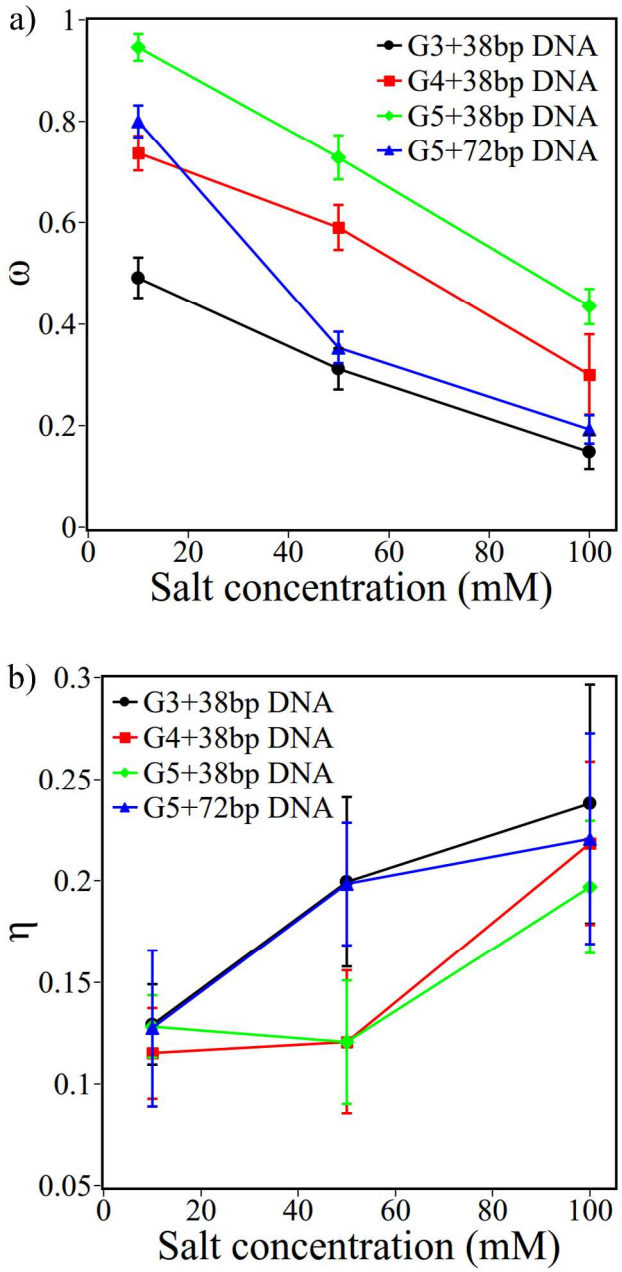

Fig.8 a) Fraction ω of adsorbed DNA phosphate beads and b) order parameter η in dendrimer – DNA complexes as functions of salt concentration. The error bars represent standard deviations taken over 500 sampling points of the simulation.

Since a dendrimer can induce global bending of DNA double strands through strong electrostatic interactions, it can also alter the local structure of DNA or even disrupt the DNA complementary base-pairs. To quantify this effect, we measured the DNA base-pair denaturing ratios (1-Φ) over 500 sampling points, which were taken every 1×10^4 MCS after equilibration. We define denaturation, or hydrogen-bond breakage, as occurring when the distance between the two complementary base beads becomes larger than (σ_{bi}+2.0 Å). The results are presented in Fig. 9, where the error bars are the standard errors of those 500 sampling points. The denaturation fraction for a 38 bp DNA double-strand is larger than for a 72 bp DNA, because the melting temperature of a short DNA molecule is lower than that of a long one, and all our simulations were carried out at the same temperature. More complementary base-pairs denature in the DNA molecules condensed by the dendrimer than in free DNAs because of bending induced by the dendrimer. Note that all these denaturation ratios were around 0.1. Therefore, although the bending or distortion introduced by dendrimers bound to the DNA might cause local base-pair melting, this DNA denaturing is not strong for salt concentrations ranging from 10 mM to 100 mM. This finding perfectly agrees with our previous circular dichroism (CD) experiments[6] showing that DNA molecules remain in the classical B-form in dendrimer – DNA complexes. Unlike some other synthetic nanoparticles[37], no strong hydrophobic force exists between dendrimer and DNA bases. Therefore, PAMAM dendrimer can condense the dsDNA effectively without disrupting the local complementary base-pair structure, as confirmed by our simulations.

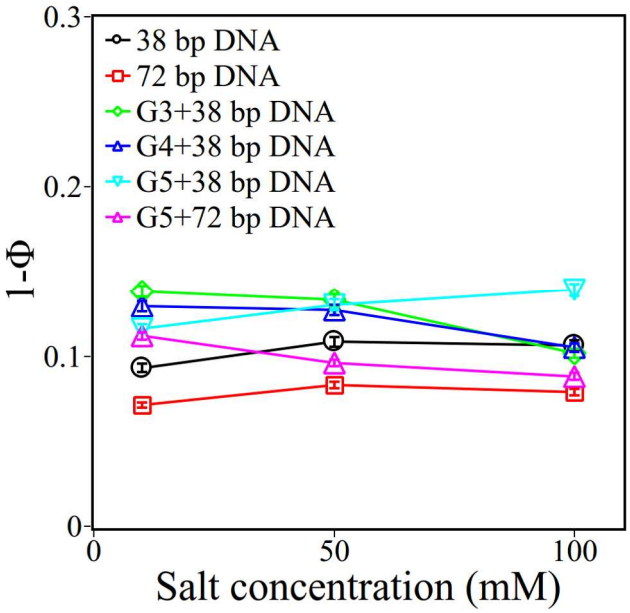

Fig. 9 Fraction of base-pair denaturation of free DNAs or DNAs condensed by dendrimer molecules as a function of salt concentration. The small error bars shown are the standard errors of the mean.

Dendrimer surface charge density effects

One of our objectives in developing this CG model of dendrimer – DNA complexation is to investigate how the surface charge density of a dendrimer affects the condensed dsDNA structure with improved resolution over earlier results that used more coarse-grained models.[13-15] By varying pH or salt concentration, the interaction between DNA and the dendrimer can be changed significantly. However, changing pH or salt concentration might also change DNA structure, which is not captured in DNA models that do not include base-pairing, such as effectively single-strand polyelectrolyte models. More importantly, to condense or compact DNA molecules for gene delivery, the range of pH and of salt concentration is constrained to avoid cell damage. Thus, modifying the surface charge density of a dendrimer, or more

generally, any DNA carrier, through acetylation or PEGylation, can be a better method of controlling macroion – DNA interaction, than adjusting pH or salt concentration.

Here we only consider acetylation. But as discussed recently,[38] it is easy to extend our model to study PEGylated dendrimer – DNA interactions. As discussed above, here we account for acetylation of a dendrimer terminal group by simply randomly "switching off" the dendrimer terminal bead charges with probability corresponding to the fraction of neutralized charges. The radii of gyration (R_g), adsorption ratios (ω), and order parameters (η) were obtained by averaging over three independent runs for each acetylation ratio. Because charges of dendrimer terminal beads were randomly set to zero, there were different numbers of charges on the dendrimer in each of the three simulations. This allows us to account for dispersion in properties of the complexes (e.g., R_g) due to non-uniformity in dendrimer charge, which is present in experimentally synthesized dendrimers.

Average properties as well as standard deviations of acetylated G5 complexes at 10 mM salt concentration are plotted in Fig. 10. As shown in Fig. 10a, the R_g of the complex increases with the acetylation fraction, as a result of decreasing dendrimer-DNA attraction. However, the R_g of the complex increases very slowly when the acetylation is less than 40%, but it increases rapidly above about 50%. This R_g vs. acetylation curve explains well our dynamic light scattering results[6] that only when the acetylation is less than 50% is there a clear one-peak relaxation time distribution of the dendrimer – DNA complex. When the acetylation of the dendrimer was larger than 50%, two peaks in the relaxation time distribution were observed, similar to that of free DNA, with no dendrimer present at all. The two peaks represent the internal motion and translational motion of the free DNA or of the complexes. The persistence of these two peaks for DNA interacting with highly acetylated dendrimers implies that, rather than strongly condense

DNA, weakly charged G5 dendrimers only slightly bend DNA double strands, as predicted by our CG model, thereby allowing DNA to retain its internal motion.

As discussed above, in 10 mM salt, adsorbed DNA phosphate beads neutralize the positive surface charges of the dendrimer. As a result, the fraction of DNA adsorption decreases almost linearly as dendrimer acetylation increases, as shown in Fig. 10b.

As shown in Fig. 10c, the order parameter η for dendrimers acetylated to different extents remains higher than 0.05, which indicates that 72bp dsDNA curves around the dendrimer. The order parameter η increases as acetylation increases from 30% to 90%, but is constant for the less acetylated dendrimers, for which we report two values of the order parameter in Fig. 10c, to be discussed in the next section.

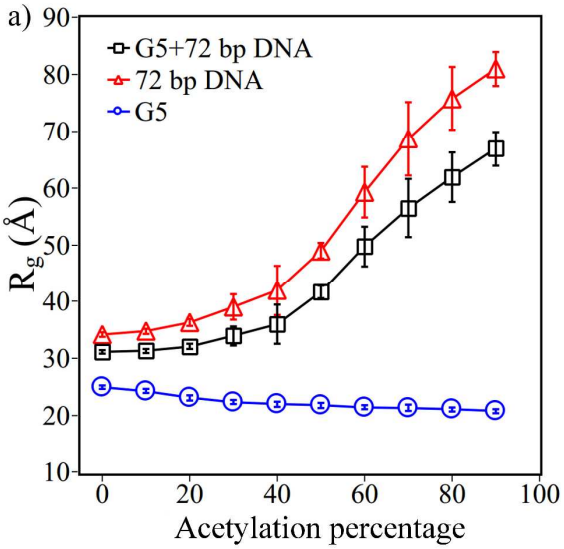

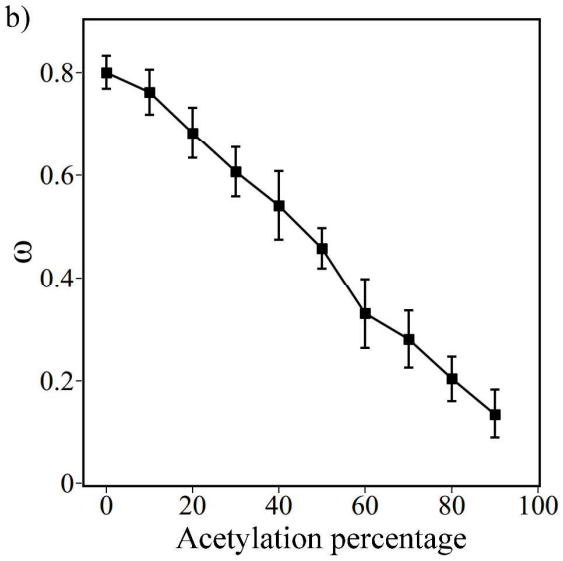

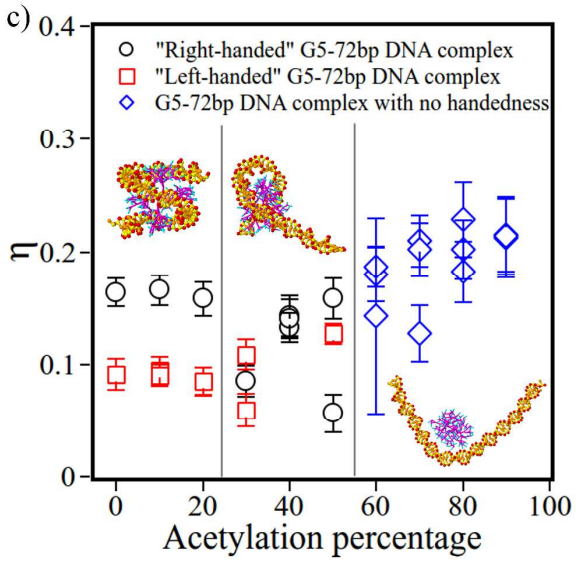

Fig. 10 a) Radius of gyration of DNA, dendrimers, and complexes vs. acetylation fraction at 10 mM salt. b) Adsorption fractions of DNA phosphate beads onto dendrimer surface and c) order parameters of DNA in dendrimer – DNA complexes. (The error bars are standard deviations.)

Handedness of DNA – dendrimer complexes

Complexes between DNA and any high generation (>5) dendrimer are unlikely to achieve the global free energy minimum because of strong electrostatic attraction, which makes it difficult for the complexes to explore configurational space and escape local free energy minima. However, for a fully charged G5 dendrimer interacting with a 72 bp DNA, after equilibration at 10 mM salt concentration, we observe that the complex eventually relaxes to either a "left-handed" (Fig. 11a) or a "right-handed" (Fig. 11b) superhelix. Although in these complexes, DNA lengths are only half that in a nucleosome, the complex structures seemed to be the similar to those in a nucleosome. However, the DNA supercoiling in a nucleosome is left-handed, as resolved by Luger et al,[39] although recent research has revealed that the right-handed nucleosome can sometimes exist both *in vitro* and *in vivo*.[40] The mechanism of chirality selection in the nucleosome is still not fully understood, especially since simulations of nucleosome assembly from free DNA and histones remains very challenging.

Our CG simulations of dendrimer – DNA complexes suggest that macroions with no chirality, such as dendrimers, are not able to compact DNA into superhelices with a specific handedness, although the wrapping energy might not be completely symmetric, because of the chirality of DNA. In fact, we find that the order parameter η of the left-handed wrapping is 0.09±0.01, while η for the right-handed complex is 0.16±0.01 (errors are standard deviations) for dendrimers acetylated to 20% or less, as shown in Fig. 10c. When the acetylation ratio is high (>50%), the dendrimer adheres poorly to DNA, so that the complexes have no handedness. At intermediate

acetylation (between 20% and 50%), the handedness of the DNA wrapping can be discerned, but the wrapping is incomplete and fluctuating, leading to a fluctuating order parameter, as indicated by the results in Fig. 10c.

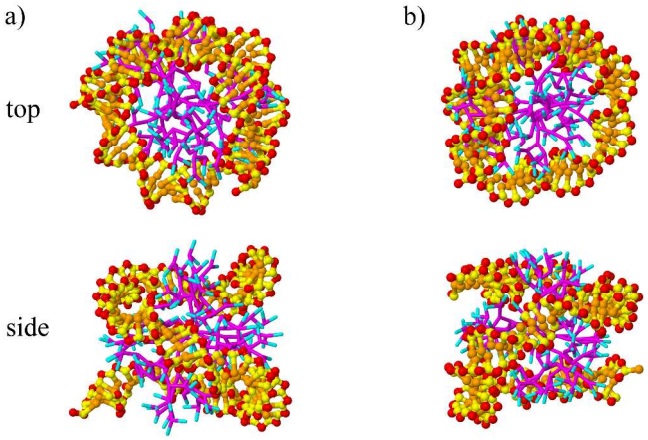

Fig. 11 a) "Left-handed" G5 dendrimer – 72 bp DNA complex. b) "Right-handed" G5 non-acetylated dendrimer – 72 bp DNA complex (at 10mM salt concentration).

Multiple dendrimers on one DNA

Since no periodic boundary conditions are applied in any of our simulations and so we have no box size limitations, we can study spatially extended structures, so as two dendrimers interacting with a single DNA molecule to assess dendrimer-dendrimer interactions along the DNA. To compare results for dendrimers of different generation, we choose three systems with the same r_{charge}, as shown in Fig. 12. The radius of gyration of a G3 dendrimer is only about 1.6 nm, less than the diameter of dsDNA, which is about 2.2 nm. Therefore, in a G3 – DNA complex, the DNA molecules tend to remain linear (see Fig. 12a) because of the repulsion between DNA segments as well as the repulsion between the two G3 dendrimers. In a G4 – DNA complex, on the other hand, the DNA can form a zig-zag structure (see Fig. 12b), and remains in the same plane. Since the R_g of the G5 dendrimer is larger than the diameter of DNA, the DNA can cover a larger fraction of the G5 surface than of the G3 surface. Thus, a nucleosome-like complex can

form, as shown for the G5 complex in Fig. 12c. These results show the differences in the local structure of complexes between dendrimers of different generation for the same values of r_{charge}. These results are a starting point to help explain the differences in structure of the much larger complexes formed experimentally when DNA is condensed by dendrimers of different generation at the same r_{charge}, as observed under cryo-TEM.[2] In particular, for large dendrimers, such as G6, large globular aggregates of size 100 nm are observed, while for smaller G4 and G2 dendrimers, a transition occurs to folded bundles and eventually toroids. The structures we see in simulations might be the precursor sub-structures that assemble into the larger experimental structures, with the more linear and planar structures seen for G3 and G4 in Fig. 12a&b assembling into bundles or toroids, while the globular structures formed by G6 in Fig. 12c might condense into large globular aggregates. Of course, this is speculation at this point, but the results presented here at least point the direction for further work to determine the hierarchy of structures formed by DNA/dendrimer complexes, and their possible analogies to the hierarchies present in DNA/histone structures. A good future step would be to design a coarse-grained model that predicts correctly the two-dendrimer/DNA structures shown in Fig. 12, but is cheap enough to simulate complexes formed by much longer DNA interacting with many dendrimers.

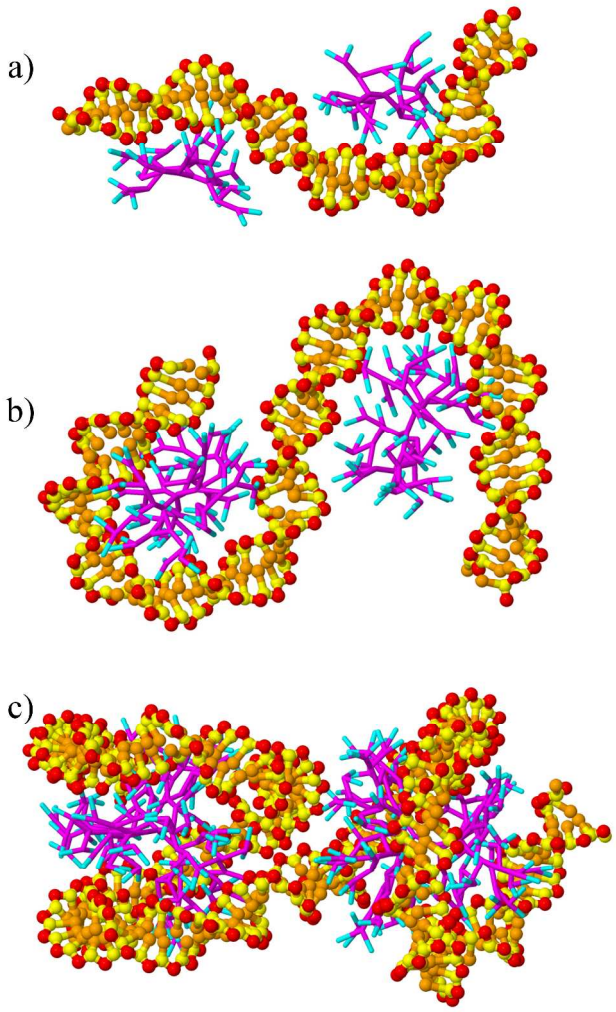

Fig. 12 a) Two G3 dendrimers on a 36 bp DNA; b) two G4 dendrimers on a 72 bp DNA; and c) Two G5 dendrimers on a 144 bp DNA.

CONCLUSIONS AND FUTURE WORK

We combined the 3SPN.1 course-grained (CG) DNA model of de Pablo [1] with the CG dendrimer model of Welch and Muthukumar,[13] to define a hybrid CG model that can be used to simulate PAMAM dendrimer – DNA complexes much more rapidly than possible for atomistic simulations, but with resolution of the double helical structure of DNA. Using this CG model, we were able to investigate the effect of dendrimer generation, salt concentration, and dendrimer surface charge density on the structure of the complex. Our simulations confirm that at low salt

concentration (10 ~100 mM) PAMAM dendrimers of various generation are able to condense dsDNA significantly without disrupting the local DNA double helix structure, in agreement with experimental studies.[2] But when the number of charges on the dendrimer are reduced to less than 10 by acetylation, at least for generation G5, the dendrimer no longer induces DNA wrapping, but merely attaches to the DNA. A similar transition from strong to weak DNA attachment has been observed as the number of charges is reduced to below 15 or 10, for other condensing agents, including charged nanoparticles[37] and polyelectrolytes.[41] The structure of the complex depends strongly on both the charge and size of the dendrimer. A fully charged G5 dendrimer at low salt (10 mM) is wrapped by DNA as in the nucleosome, but with either left- and right-handed DNA superhelices. The simulation method is fast enough to simulate pairs of dendrimers binding to a single long DNA strand, which begins to mimic the smallest scales of chromatin-like structures. The use of accelerated Metropolis schemes using cluster moves, faster simulation methods, faster computers, and/or coarser-grained models tuned to capture the effects reported here, should open the door to simulating larger structures containing multiple dendrimers and longer pieces of DNA. This new CG model can also easily be extended to other interesting polyelectrolytes[37,41,42] as well as dendrimers with different surface modifications.[38] Using a coarse-grained protein model with appropriate resolution,[43] and a new version of the 3SPN force field recently incorporated into LAMMPS,[20] the model could be adapted to simulate the dynamics of protein – DNA binding, including the initial phases of chromatin formation. Since electrostatic interactions in our simulations are estimated using the Debye-Hückel theory, our model has limitations and likely becomes inaccurate at high salt concentrations. Nevertheless, a mesocale model with a resolved DNA double helix, combined with mesoscale models of large

condensing agents could be very helpful to understand cationic macroion/DNA interaction generally, as suggested by our simulations.

ACKNOWLEDGMENTS

We thank Dr. Ioan Andricioaei and Emel Ficici for insightful discussions. We acknowledge support from NSF under grant EFRI 0938019. Any opinions, findings, and conclusions or recommendations expressed in this material are those of the authors and do not necessarily reflect the views of the National Science Foundation (NSF).

REFERENCE

1. E. J. Sambriski, D. C. Schwartz, and J. J. de Pablo, *Biophys. J.*, 2009, **96**, 1675–1690.
2. M.-L. Ainalem, A. M. Carnerup, J. Janiak, V. Alfredsson, T. Nylander, and K. Schillén, *Soft Matter*, 2009, **5**, 2310–2320.
3. A. M. Carnerup, M.-L. Ainalem, V. Alfredsson, and T. Nylander, *Langmuir*, 2009, **25**, 12466–12470.
4. R. Dootz, A. C. Toma, and T. Pfohl, *Soft Matter*, 2011, **7**, 8343–8351.
5. M.-L. Orberg, K. Schillén, and T. Nylander, *Biomacromolecules*, 2007, **8**, 1557–1563.
6. S. Yu, M. Li, S. K. Choi, J. R. Baker, and R. G. Larson, *Molecules*, 2013, 10707–10720.
7. K. Wada, H. Arima, T. Tsutsumi, Y. Chihara, K. Hattori, F. Hirayama, and K. Uekama, *J. Control. Release*, 2005, **104**, 397–413.
8. H. Crampton and E. Simanek, *Polym. Int.*, 2007, **496**, 489–496.
9. A. M. Carnerup, M.-L. Ainalem, V. Alfredsson, and T. Nylander, *Soft Matter*, 2011, **7**, 760–768.
10. X. Wang, Y. He, J. Wu, C. Gao, and Y. Xu, *Biomacromolecules*, 2009, 245–251.
11. B. Nandy and P. K. Maiti, *J. Phys. Chem. B*, 2011, **115**, 217–230.
12. M. Mills, B. Orr, M. M. Banaszak Holl, and I. Andricioaei, *Biophys. J.*, 2010, **98**, 834–842.
13. P. Welch and M. Muthukumar, *Macromolecules*, 2000, **2**, 6159–6167.

14. S. V. Lyulin, A. A. Darinskii, and A. V. Lyulin, *Macromolecules*, 2005, **38**, 3990–3998.

15. S. V Larin, A. A. Darinskii, A. V Lyulin, and S. V Lyulin, *J. Phys. Chem. B*, 2010, **114**, 2910–2919.

16. T. Lewis, G. Pandav, A. Omar, and V. Ganesan, *Soft Matter*, 2013, **9**, 6955–6969.

17. Q. Cao, C. Zuo, Y. Ma, L. Li, and Z. Zhang, *Soft Matter*, 2011, **7**, 506–514.

18. A. Savelyev and G. Papoian, *Biophys. J.*, 2009, **96**, 4044–4052.

19. T. A. Knotts, N. Rathore, D. C. Schwartz, and J. J. de Pablo, *J. Chem. Phys.*, 2007, **126**, 084901.

20. D. M. Hinckley, G. S. Freeman, J. K. Whitmer, and J. J. de Pablo, *J. Chem. Phys.*, 2013, **139**, 144903.

21. V. Ortiz and J. de Pablo, *Phys. Rev. Lett.*, 2011, **106**, 3–6.

22. I. V. Dobrovolskaia and G. Arya, *Biophys. J.*, 2012, **103**, 989–998.

23. T. Schlick and O. Perisić, *Phys. Chem. Chem. Phys.*, 2009, **11**, 10729–10737.

24. G. Arya and T. Schlick, *J. Phys. Chem. A*, 2009, **113**, 4045–4059.

25. A. Stogryn, *IEEE Trans. Microw. Theory Tech.*, 1970, **19**, 733–736.

26. D. C. Rau and V. a Parsegian, *Biophys. J.*, 1992, **61**, 246–259.

27. H. Drew and R. Wing, *Proc. Nati. Acad. Sci.*, 1981, **78**, 2179–2183.

28. S. Kumar, J. Rosenberg, D. Bouzida, R. Swendsen and P. Kollman, *J. Comput. Chem.*, 1992, **13**, 1011–1021.

29. Y. Liu, V. S. Bryantsev, M. S. Diallo, and W. A. Goddard, *J. Am. Chem. Soc.*, 2009, **131**, 2798–2799.

30. P. K. Maiti, T. Çağın, G. Wang, and W. A. Goddard, *Macromolecules*, 2004, **37**, 6236–6254.

31. P. K. Maiti, T. Çağın, S.-T. Lin, and W. A. Goddard, *Macromolecules*, 2005, **38**, 979–991.

32. H. Lee, J. R. Baker, and R. G. Larson, *J. Phys. Chem. B*, 2006, **110**, 4014–4019.

33. T. Prosa and B. Bauer, *J. Polym. Sci. Part B Polym. Phys.*, 1997, **35**, 2913–2924.

34. K. Fant, E. K. Esbjörner, A. Jenkins, M. C. Grossel, P. Lincoln and B. Norden, *Mol. Pharm.*, 2010, **7**, 1734–1746.

35. P. E. Theodorakis, H-P Hsu, W. Paul and K. Binder, *J. Chem. Phys.*, 2011, **135**, 164903.

36. T. Sakaue, K. Yoshikawa, S. Yoshimura, and K. Takeyasu, *Phys. Rev. Lett.*, 2001, **87**, 078105.

37. J. G. Railsback, A. Singh, R. C. Pearce, T. E. McKnight, R. Collazo, Z. Sitar, Y. G. Yingling, and A. V Melechko, *Adv. Mater.*, 2012, **24**, 4261–4265.

38. T. Zhou and S. B. Chen, *Macromolecules*, 2005, **38**, 8554–8561.

39. K. Luger, A. Mader, and R. Richmond, *Nature*, 1997, **389**, 251–260.

40. C. Lavelle, *EMBO Rep.*, 2009, **10**, 1185–1186.

41. T. Akitaya, A. Seno, T. Nakai, N. Hazemoto, S. Murata, and K. Yoshikawa, *Biomacromolecules*, 2007, **8**, 273–278.

42. K. Schille and T. Nylander, *Phys. Chem. Chem. Phys*, 2004, 1603–1607.

43. Q. Zhang, D. a Beard, and T. Schlick, *J. Comput. Chem.*, 2003, **24**, 2063–2074.